Fire Safety Journal 162 (2026) 104753

Contents lists available at ScienceDirect

Fire Safety Journal

journal homepage: www.elsevier.com/locate/firesaf

A unified scaling law for bushfire junctions

Ahmad Hassan [a,*], Gilbert Accary [b], Jason Sharples [c], Khalid Moinuddin [a]

[a] Victoria University, Melbourne, Australia
[b] Lebanese American University, Byblos, Lebanon
[c] University of New South Wales, Canberra, Australia

ARTICLE INFO

Keywords:
Merging wildfires
Physics-based wildfires modelling
Large-eddy simulation
FIRESTAR3D
Fire-induced wind

ABSTRACT

The study of extreme fire phenomena is limited by the experimental capabilities, especially in terms of geometric scale. Scaling tools provide a solution to extrapolate limited laboratory-scale results to large real-world-scale scenarios. In this paper, a new scaling law is proposed for merging bushfires (which propagate quasi-steadily) through a relationship between the normalised rate of spread of junction fire and Byram's convective number. The proposed law accounts for wind and slope effects, highlighting the role played by the two forces governing the flame-front dynamics and the plume trajectory: buoyancy force and wind inertia. A large set of numerical simulations of the junction fire at a wide range of scales, slopes, wind speeds, junction angles and two types of fuel (grass and shrub) was carried out using fully physical modelling. Results show that the normalised rate of spread of a junction fire depends only on a modified expression of Byram's convective number and on fuel type. Moreover, the proposed expression of Byram's number yields a unified scaling law for both junction fires and single straight fire lines for quasi-steady fires. The research helps assess the effects of some topographical parameters in extreme fires, improving situational awareness, operational predictions and firefighter safety.

1. Introduction

Junction fires are the extreme bushfire merging events that occur when two or more flame fronts converge at a certain angle (called junction angle) and are recognised as one of the most dangerous and least understood forms of extreme fire behaviour [1]. Early laboratory-scale studies showed that junction fires spread fast because heat accumulates near the vertex where the two junction arms meet, rather than being carried mainly along a single front [1]. At the junction point, the rate of spread (ROS) often exceeds that of the individual fire-lines prior to merging, creating a junction effect (i.e., ROS surplus) that can rapidly escalate fire spread [2]. The smaller the junction angle, the stronger is the junction effect [3]. This sudden fire acceleration poses significant risks for fire suppression operations and requires improved predictive capability at various field scales, especially with the high risk of fire eruption. Dimensional analysis of junction fire would help quantify the phenomenon and unify behaviour patterns.

Indeed, dimensional analysis is widely regarded as one of the most effective methods in physics. It provides a systematic framework for designing laboratory experiments that reproduce large-scale physical phenomena on a reduced scale. Beyond its practical role in experimental design, it also offers insight into the fundamental processes that govern the behaviour of complex physical systems. A key strength of similitude theory lies in its ability to collapse data from different scales and conditions onto a single curve. This makes it possible to justify the study of problems at laboratory scale when large-scale testing is unfeasible or too costly. For further reading, see standard Fluid Mechanics references such as Fox, McDonald, and Pritchard [4].

Early bushfire studies [5–7] showed that fire spread depends mainly on the interplay between wind inertia and buoyancy resulting from plume-air density differences. Byram [5] proposed in 1959 that the balance between buoyancy and wind forces could serve as a basis for predicting fire behaviour. For fires spreading in vegetation over level ground, Byram introduced a dimensionless parameter, later termed Byram's convective number, defined as the ratio of buoyancy power to wind power per unit area. This parameter, expressed in Eq. (1), incorporates fire intensity (I), air properties (density ρ, specific heat at constant pressure C_P, and ambient temperature T_0), earth gravitational

This article is part of a special issue entitled: FISJ_IAFSS 2026 published in Fire Safety Journal.

* Corresponding author.
E-mail addresses: ahmad.hassan6@live.vu.edu.au (A. Hassan), gilbert.accary@lau.edu.lb (G. Accary), j.sharples@unsw.edu.au (J. Sharples), khalid.moinuddin@vu.edu.au (K. Moinuddin).

https://doi.org/10.1016/j.firesaf.2026.104753
Received 24 September 2025; Received in revised form 13 February 2026; Accepted 18 March 2026
Available online 21 March 2026

acceleration g, the ROS R, and the wind velocity component (U_W) at a reference height (typically 10 m at field scale and 1 m at laboratory scale) aligned with fire propagation direction. Byram's convective number can be reformulated using the vertical velocity of the thermal plume above the fire U_B [8] given by Eq. (2).

$$N_C = \frac{2gI}{\rho C_P T_0 (U_W - R)^3} = \frac{\frac{1}{2}\rho U_B^3}{\frac{1}{2}\rho (U_W - R)^3} \tag{1}$$

$$U_B = \left(\frac{2gI}{\rho C_P T_0}\right)^{1/3} \tag{2}$$

Nelson [9] revisited the threshold criteria originally proposed by Pagni and Peterson [7] to define fire spread regime, expressing them in terms of Byram's convective number. According to this formulation:

- For $N_C \leq 2$, the fire is wind-driven, with flame behaviour governed mainly by the wind and fire spread dominated by convection heat transfer.
- For $N_C \geq 10$, the fire becomes plume-dominated, where buoyancy controls the flame trajectory and radiative transfer dominates fire spread.
- For $2 < N_C < 10$, the fire exhibits a mixed regime, transitioning between wind-driven and plume-dominated behaviour.

Morvan and Frangieh [10] carried out a similitude analysis (using experimental data and numerical simulation results) and showed a scaling between Byram's convective number and the ratio R/U_w. The analysis indicated that at small values of N_C (wind-driven fires), the ratio R/U_w tends towards a constant value, while for large values of N_C (plume-dominated fires), R/U_w increases with N_C.

Nelson also extended the expression of Byram's convective number to include slope effects, generalising its use beyond flat terrain [9]. This expression was then revisited by Morvan and Accary [11] in order to properly account for the slope effect in Byram's convective number, by projecting the buoyancy characteristic velocity U_B in two orthogonal directions: parallel and normal to the direction of fire propagation, as illustrated in Fig. 1. The expression of Byram's number proposed by Morvan and Accary [11] is given by Eq. (3), where α is the slope angle and U_e is the effective wind speed acting in the fire propagation direction.

$$N_C = \frac{\frac{1}{2}\rho U_B^3 \cos^3\alpha}{\frac{1}{2}\rho (U_e - R)^3} = \frac{2\,g\,I\,\cos^3\alpha}{\rho C_P T_0 (U_e - R)^3} \text{ with } U_e = U_W + U_B \sin\alpha \tag{3}$$

Following Morvan and Frangieh's work [10] and relying on experimental data and numerical simulations of fire spread on a sloping terrain, a scaling was again found between Byram's convective number and the ratio R/U_e, with a clear change in the scaling law at the transition between wind/slope-driven fire and plume-dominated one [11].

This analysis carried out for a single fire-line on a sloping terrain is extended in this paper to junction fires. Junction fires exhibit non-linear behaviour driven by the interaction of wind, slope, and junction angle [12]. As in the case of a single straight fire front, the dynamics of junction fires is governed by the competition between buoyancy-driven convection and wind-driven inertia, reflected by Byram's convective number. The geometry of the junction (mainly characterised by the junction angle) is an additional parameter governing the interaction of two junction arms and affecting the components of the prevailing wind speed and of the vertical velocity of the thermal plume acting on the junction arms.

In this paper, a scaling for the normalised junction fire ROS (R/U_e), based on a modified expression of Byram's convective number (that explicitly incorporates wind, slope, and junction angle dependencies) is proposed for junction fires. Then, using fully physical modelling, a comprehensive set of 130 simulations, conducted across multiple scales, fuels, wind speeds, slopes, and junction geometries was performed. However, results of 55 quasi-steady cases are reported. The analysis identifies key parameters that govern junction fire behaviour, and the proposed scaling law is tested, providing a means to bridge the gap between laboratory-scale experiments (where scale and fire intensity are constrained) and large-scale or real-world junction fire scenarios. By integrating junction fire physics, scaling theory, and the quantification of ROS surplus into a unified framework, this work advances both the theoretical understanding and operational prediction of extreme fire behaviour, supporting improved firefighter safety and decision-making in complex bushfire environments.

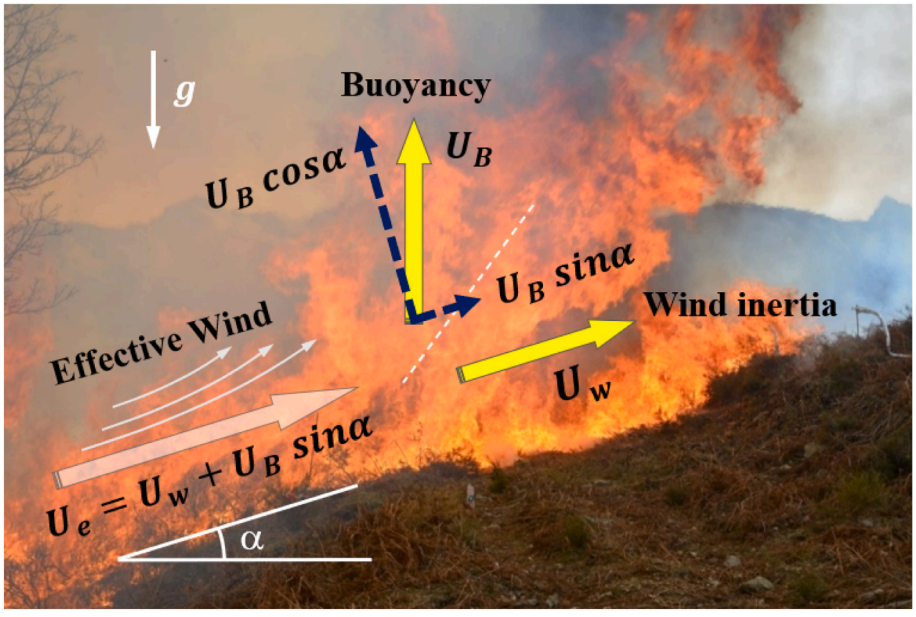

Fig. 1. Forces governing bushfire behaviour on a sloping terrain: wind inertia (parallel to the ground), buoyancy (vertical) having two components that are parallel and normal to the direction of fire propagation.

2. Junction-fires scaling

We consider the idealised, symmetric, junction fire configuration shown in Fig. 2, where the prevailing wind speed U_W acting in the junction axis direction, the slope angle α, the junction angle θ, and the junction arm length L_0 are the main control parameters. As long as the angle between the junction arms is conserved during fire spread, the ROS of the junction point R_{JP} is related to the ROS of the junction arm in the normal direction to the arm R_{JA} through a simple geometric relation given by $R_{JA} = R_{JP} \sin(\theta_{½})$, where $\theta_{½}$ is half the junction angle θ.

As in the case of a straight fire line, the propagation of the junction arm in the normal direction to the arm depends on the competition between the components of the prevailing wind speed and of the vertical velocity of the thermal plume acting in two orthogonal directions: parallel and normal to the direction of the junction arm propagation. The component of the prevailing wind speed acting in the direction of the arm propagation is $U_W \sin(\theta_{½})$, while the components of the thermal-plume vertical velocity U_B are shown by Fig. 3. U_B has two relevant components for the junction arm propagation: $U_{B,a} = U_B \sin(\alpha) \sin(\theta_{½})$ acting in the junction arm propagation direction and $U_B \cos(\alpha)$ acting in the normal direction to the junction arm propagation direction. The third component of U_B, which is parallel to the junction arm and equal to $U_B \sin(\alpha) \cos(\theta_{½})$, would not affect the propagation of the junction arm. Consequently, the effective wind speed acting in the propagation direction of the junction arm is given by Eq. (4).

$$U_{e,a} = U_W \sin(\theta_{½}) + U_B \sin(\alpha)\sin(\theta_{½}) \tag{4}$$

It should be noted that $U_{e,a} = U_e \sin(\theta_{½})$, where U_e is the effective wind speed acting in the junction point propagation direction (the x direction) and given by Eq. (3). By analogy to a single straight fire-line spreading on a sloping terrain [11], we define Byram's convective number based on the junction arm parameters according to Eq. (5), where I_a is the junction fire arm intensity.

$$N_{C,a} = \frac{\frac{1}{2}\rho U_B^3 \cos^3\alpha}{\frac{1}{2}\rho\left(U_{e,a} - R_{JA}\right)^3} = \frac{2\,g\,I_a \cos^3\alpha}{\rho C_P T_0 \left(U_{e,a} - R_{JA}\right)^3} \tag{5}$$

By analogy to a single straight fire-line [10,11], a scaling is expected between Byram's convective number $N_{C,a}$ (based on the junction arm parameters) and the normalised ROS of the junction arm $R_{JA}/U_{e,a}$. It should also be noted that, since $R_{JA} = R_{JP} \sin(\theta_{½})$ and $U_{e,a} = U_e \sin(\theta_{½})$, the same scaling would be expected between $N_{C,a}$ and the normalised ROS of the junction point R_{JP}/U_e.

The existence of such scaling is tested using a set of 55 out of 130 numerical simulations carried out using a fully physical, computational fluid dynamics (CFD), fire simulator, FIRESTAR3D for different control parameters (junction angle θ, slope angle α, prevailing wind speed U_W), for two fuel types (grass and shrub), and at different length scales. The aim is to obtain a unified, dimensionless scaling law for all cases despite any diversity of scale, conditions, fuel type, slope, geometry and various other parameters that can potentially affect the junction fire behaviour.

3. Numerical model

FIRESTAR3D is a fully physical, CFD model based on a multiphase formulation [13,14]. The model predicts the behaviour of the coupled system consisting of a turbulent-reactive gaseous flow (fluid phase) interacting with a plant canopy (solid phase) modelled as a porous medium. The evolution of each phase is governed by a set of conservation equations with source/sink terms representing the interaction between the two phases. The mathematical model of the fluid phase consists of the conservation equations of mass, momentum, energy and chemical species resulting from vegetation decomposition. The model is solved using the standard finite volume method on a structured mesh; the method is third-order accurate in space and time. Because it uses a fully implicit time scheme, the code is unconditionally stable; the time step is chosen as a fraction of the characteristic time of the underlying physics. The radiation transfer equation is solved using the Discrete Ordinate Method (DOM) or SN approximation; the reported simulations were performed using S8 approximation. The code employs a large-eddy simulation (LES) turbulence model and radiation turbulence interaction model [14]. Combustion in the gaseous phase is based on CO kinetics, using an Eddy Dissipation Concept model to evaluate the combustion rate occurring in the gaseous phase [13]. The fourth-order Runge-Kutta method is used to solve (on an independent grid) the solid-phase model describing the decomposition of the vegetation as a result of the intense heat flux coming from the flaming zone [14]. The degradation of the vegetation is governed by three temperature-dependent mechanisms: drying, pyrolysis, and charcoal combustion. The constants of the model associated with the charcoal combustion (activation energy and pre-exponential factor) are evaluated empirically from a thermal analysis conducted on various solid fuels samples [13]. FIRESTAR3D model has been extensively validated using various configurations of bushfire spread, both at laboratory and field scales, both with shrub and grass [13,15]. In particular, for the configuration of a junction fire, the model has been validated [16–18] using data collected from laboratory experiments [2].

Fig. 4 shows the junction fire configuration and the computational domain considered in this study. A V-shaped homogeneous fuel-bed layer is considered on inclined terrain making an angle α with the

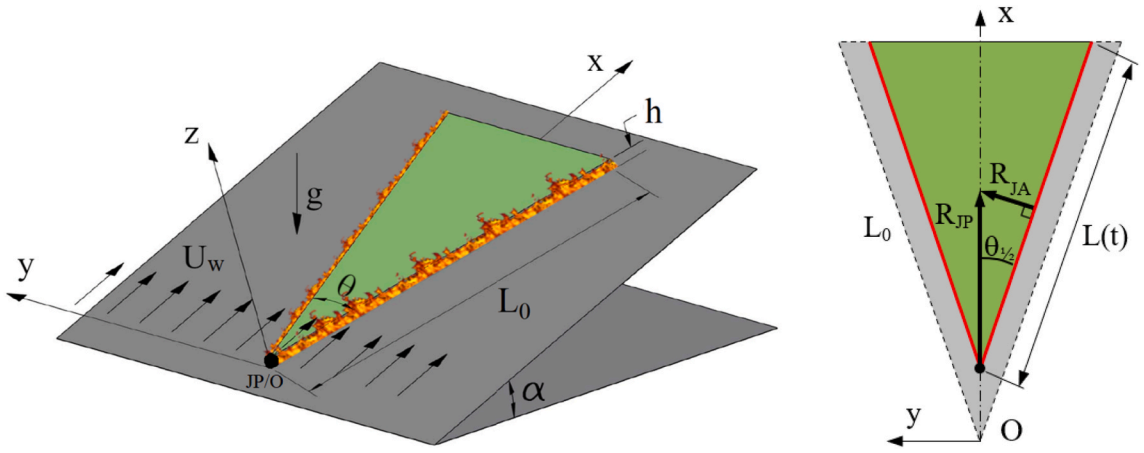

Fig. 2. Isometric (left) and top (right) views of a junction fire and geometric parameters. α is the slope angle, θ is the junction angle ($\theta_{½} = \theta/2$), U_W is the prevailing wind speed, L_0 and L(t) are respectively the initial and the instantaneous junction arm length, R_{JP} is the junction point ROS, and R_{JA} is the junction arm ROS in the normal direction to the arm.

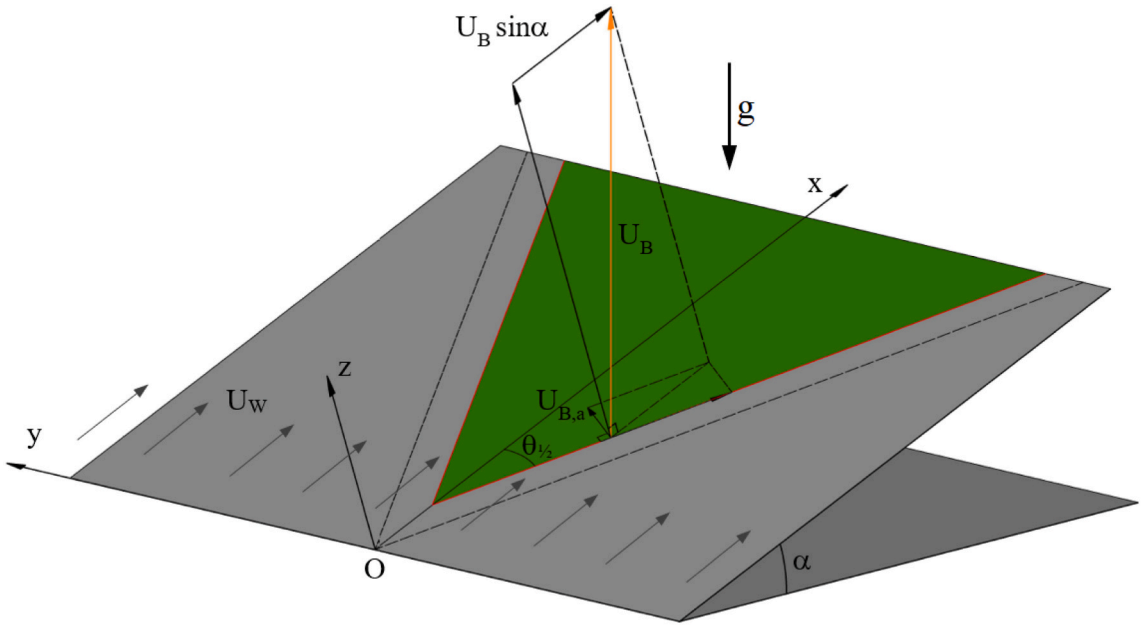

Fig. 3. Components of buoyancy characteristic velocity in a junction fire. $U_{B,a} = U_B\ sin(\alpha)$. $sin(\theta_{½})$ is the component acting in the normal direction to the junction arm in the (x,y) plane.

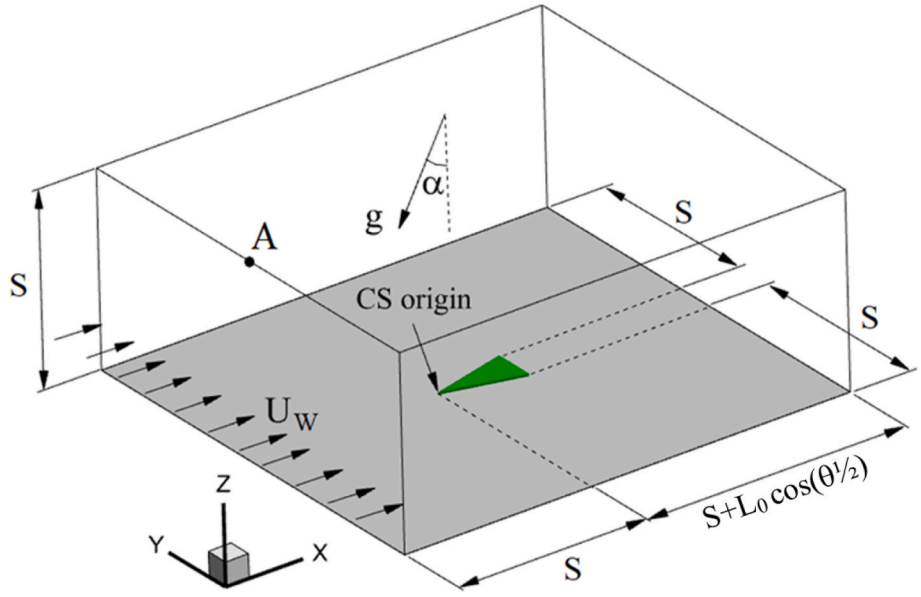

Fig. 4. Computational domain used to simulate junction fire. CS: coordinate system. *S* depends on the considered junction fire scale; for instance, S = 12 m at laboratory scale for a junction arm length L_0 = 5 m.

horizontal plane. Terrain inclination was accounted for by considering two gravity components: $g_z = -g\ cos(\alpha)$ and $g_x = -g\ sin(\alpha)$. Open boundary conditions were applied to all sides of the computational domain except the bottom one, where a solid-wall condition was imposed. The simulations were conducted for two fuel types: shrub is considered at laboratory scale (5 m $< L_0 <$ 25 m) and grass is considered at field scale (35 m $< L_0 <$ 100 m); the properties of these fuels, summarised in Table 1, were inspired by previous experimental and numerical studies [2,15,16].

Before ignition, a standard one-seventh power-law velocity profile given by Eq. (6) was applied at the inlet (with z_0 = 1 m at laboratory scale and z_0 = 10 m at field scale) resulting in the desired prevailing wind speed U_W, with 10% turbulence intensity, while Neumann conditions (i.e., zero normal-gradient) were applied at the open boundaries.

Table 1
Properties of fuels used in the numerical simulations. σ_S is the fuel surface-to-volume ratio, α_S is the packing ratio (fuel volume fraction), ρ_S is the dry fuel density, M is the fuel moisture content, h is the fuel layer thickness, C_d is the drag coefficient.

	σ_S (m^{-1})	α_S	ρ_S ($kg.m^{-3}$)	M (%)	h (m)	C_d
Shrub	6900	0.00784	500	20	0.15	0.42
Grass	4000	0.001	500	10	1	0.15

Before ignition, simulations were run long enough to reach statistically steady flow conditions.

$$U(z) = U_W \left(\frac{z}{z_0}\right)^{1/7} \quad (6)$$

Fuel is ignited by injecting *CO* at 1600 K from the bottom of the computation domain along the junction fire arms according to the procedure described in Frangieh et al. [15]. After ignition, the inlet boundary condition was modified: a Neumann condition was applied at the domain inlet (i.e., zero normal-gradient for all variables) and a pressure gradient was applied in the *x*-direction to maintain wind velocity constant far from the flaming zone (at point A in Fig. 4), while allowing the fire front to withdraw fresh air from the domain inlet. The applied pressure gradient was updated at each iteration and vanished when the velocity had reached the desired value at the specified location. This inlet condition allows for induced wind to occur at the domain inlet while maintaining the prevailing wind speed far from flaming zone [14].

A uniform mesh was used for the solid phase, while a non-uniform mesh was used for the fluid phase. Within the vegetation zone, the fluid-phase grid was uniform and then it was progressively coarsened toward the open boundaries. It should be noted that for both the fluid and the solid phases, the grid cell-size was below radiation-extinction length-scale given by $4/\alpha_S\sigma_S$ [19] and equal to about 7.4 cm for shrub and 1 m for grass. Details of the mesh structure are reported in Table 2 for a selected junction angle and scale that affect the total number of cells. Mesh sensitivity analysis for very similar simulations (mesh size, geometry, and control parameters range) was carried out in previous studies [12,16,18] and showed negligible effects on the global fire properties such as the ROS and fire intensity.

In this study, numerical simulations of junction fires were performed for a junction angle $\theta = 30°$, 60°, 90°, and 120°, for a slope angle $\alpha = 0$ (horizontal terrain), 10°, 20°, 30°, and 40°, for a prevailing wind speed $U_W = 0$ (no prescribed external wind), 0.5, 1, 2, 3, 4, 6, 10, 12 and 14 m/s, and for a junction arm length $L_0 = 5$, 10, 15 and 25 m for shrub and $L_0 = 35$, 50 and 100 m for grass. The ROS of the junction-point (R_{JP}) and of the junction-arm (R_{JA}) were computed from the temporal evolution of the fire-front position. For each case, the position of the fire front was tracked along the junction point (vertex) or the junction-arm (middle of arm). The ROS was then calculated as the average slope of the position–time curves over the steady phase of fire spread. In addition to the junction fire scenarios, a series of simulations was conducted for single, straight fire line cases in order to check the validity of the proposed scaling in this limiting case (corresponding to a junction angle of 180°) and in order to link the obtained scaling to previous works [10,11]. For these simulations, the same parameters used for junction fires (fuel types and properties, wind speed, slope angle) were considered as well as the same simulation settings (e.g., mesh size). In this case however, a rectangular vegetation layer was considered (2.5 m × 12 m for shrub and 25 m × 120 m for grass) where the long dimension was aligned with the wind and slope direction (x direction), and lateral periodic boundary conditions were used in the y direction to simulate a quasi-infinite fire front. The simulations were performed using the adaptive time-stepping strategy, with a time step between 0.001 s and 0.01 s, to maintain the L2-norm of the truncation error below 10^{-4} (in normalised form) for all transport equations. For the iterative process, the stopping criterion, based on the residuals (in L2-norm) of the transport equations, was 10^{-5} (in normalised form) or 10^{-4} (in non-normalised form). FIRESTAR3D is parallelised using OpenMP directive and the simulations were performed with 16 cores. Depending on the considered case, 3 to 9 days of CPU time are required for approximately 30 s of physical time.

Table 2
Mesh properties for a junction angle $\theta = 60°$ and for a junction fire's arm length $L_0 = 50$ m for grass and $L_0 = 5$ m for shrub. The fluid-phase cell size is reported within the fuel zone. Mesh size is expressed in number of grid-points in each direction (Nx, Ny, Nz).

	Solid-phase cell size (Δx, Δy, Δz) in (cm)	Fluid-phase cell size (Δx, Δy, Δz) in (cm)	Solid-phase mesh size	Fluid-phase mesh size
Shrub	2.5, 2.5, 1.25	5, 5, 2.5	177, 201, 13	148, 160, 160
Grass	15.625, 15.625, 6.25	31.25, 31.25, 12.5	289, 321, 17	224, 240, 150

4. Results and discussion

4.1. Assessment of fire properties

To investigate the dynamics of junction fires under combined wind and slope effects, we first analyse the evolution of the main fire parameters involved in the definition of Byram's convective number (Eq. (5)) under representative conditions. Fig. 5 shows a 3D view of a laboratory-scale junction fire, illustrating the complex flame structure formed by a sequence of crests and troughs, and highlighting the ability of FIRESTAR3D to capture such fire behaviour. The corresponding fire spread is shown in Fig. 6. The pyrolysis-front at the fuel surface is visible in Fig. 5 at the interface between the yellow (dry fuel) and black (charred fuel) regions. This front was identified by tracking the transition of the dry-fuel mass fraction from 0 to 1. The junction-point position at the fuel surface was defined as the location of the pyrolysis front along the junction axis (y = 0, z = h). On the other hand, the junction-arm position in the x-direction was determined from the pyrolysis-front location at the fuel surface along the line (y = ½ L_0 sin ($\theta_{½}$), z = h), i.e., a line parallel to the junction axis passing through the midpoint of the initial junction arm. Finally, the junction-arm length was estimated from the volume of unburned-fuel, assuming a symmetric triangular shape bounded by the two arms forming an angle θ.

Fig. 7 shows typical junction-fire spread metrics (junction-point and junction-arm propagation) obtained for shrub at laboratory scale, under separate slope and wind effects. We notice for the considered cases the existence of a quasi-steady-state of junction-fire spread, which allows the estimation of the ROS of the junction-point and of the junction-arm in the x direction from the average slope of the corresponding curves. During the initial transient phase immediately after ignition, the junction-point advances more rapidly than the junction arm; however, in the quasi-steady state their ROS values converge and remain relatively close. This behaviour supports the assumption introduced in Section 2 that the junction-arm ROS in the normal direction can be expressed as $R_{JA} = R_{JP}$ sin ($\theta_{½}$). For instance, for the two cases shown in Fig. 7, the junction-point ROS was estimated at about 21 cm/s for case 1 ($\theta = 30°$, $\alpha = 10°$, and $U_W = 0$) and at about 10 cm/s for case 2 ($\theta = 60°$, $\alpha = 0$, and $U_W = 0.5$ m/s). Fig. 7 also shows the progressive decrease in junction-arm length, which was used to evaluate the corresponding fire intensity.

To evaluate the junction-arm fire intensity I_a used in the expression of Byram's convective number, the fire heat release rate (HRR) is first evaluated from Eq. (7), where ω_{vap}, ω_{pyr}, ω_{char}, ω_{CO}, and ω_{soot} (kg/s) are the total mass rates of water evaporation, pyrolysis, char combustion, combustion of CO in the gas mixture, and soot combustion, respectively, and ΔH_{vap}, ΔH_{pyr}, ΔH_{char}, ΔH_{CO}, and ΔH_{soot} (J/kg) are the corresponding reaction enthalpies [13]. Vaporisation and pyrolysis have negative contributions in Eq. (7), since they are endothermic reactions. Note that ΔH_{char} is not constant in this case since it depends on the CO-to-CO_2 ratio produced during char combustion [13], it varies between 9 MJ/kg for incomplete combustion and 30 MJ/kg (for a complete one).

$$HRR = -\omega_{vap}.\Delta H_{vap} - \omega_{pyr}.\Delta H_{pyr} + \omega_{char}.\Delta H_{char} + \omega_{CO}.\Delta H_{CO} + \omega_{soot}.\Delta H_{soot} \quad (7)$$

For the two cases considered in Figs. 7 and 8, the HRR increases to reach a maximum, then, it globally decreases with the junction-arm length. However, by evaluating the junction-arm fire intensity (I_a) as the ratio of HRR to twice the junction-arm length, we notice in Fig. 8 that

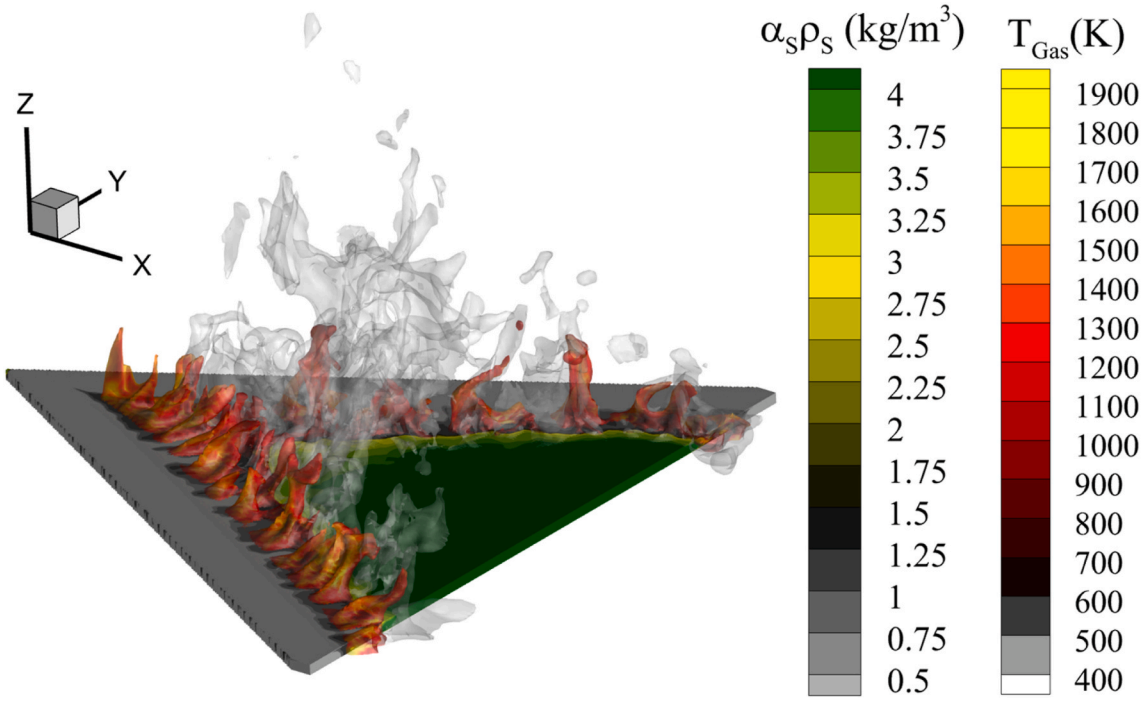

Fig. 5. 3D view of junction-fire spread obtained for shrub at laboratory scale (initial arm length $L_0 = 10$ m), 15 s after ignition, for a junction angle $\theta = 60°$, on a horizontal terrain ($\alpha = 0$), and under a prevailing wind speed $U_W = 1$ m/s. The flames are visualised using the iso-value surface of soot volume fraction of 10^{-6} coloured by the gas-mixture temperature. Combustion gases are visualised using the iso-value surface of water-vapor mass fraction of 0.01 (with 50% transparency). Fuel decomposition is visualised using fuel bulk density $\alpha_S\rho_S$.

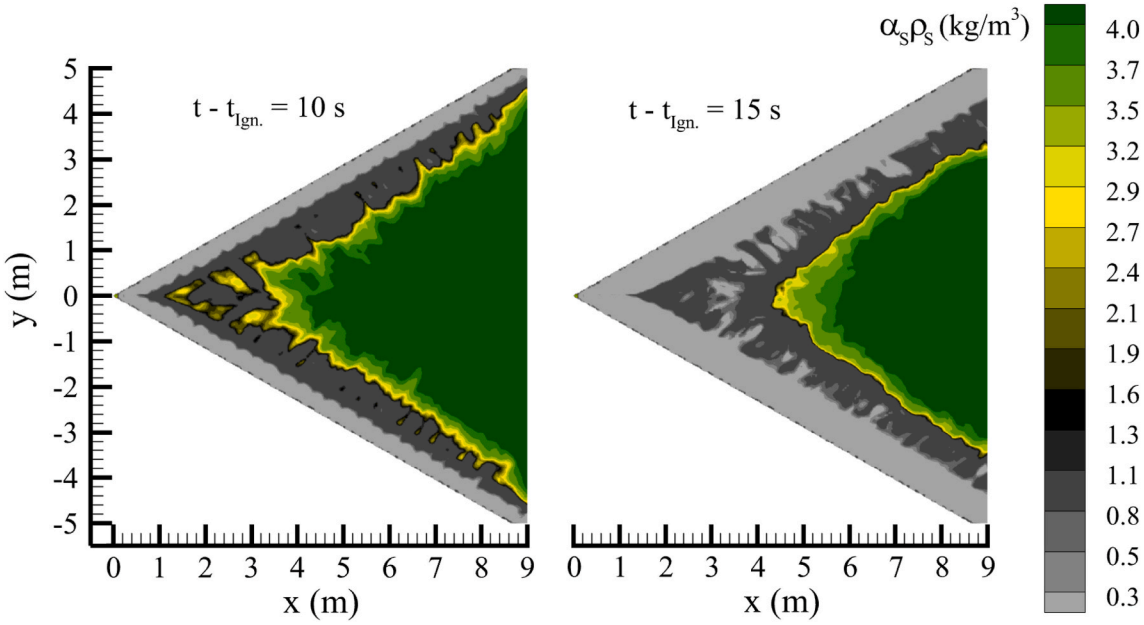

Fig. 6. Distribution of fuel bulk-density at the fuel-bed surface, obtained for shrub at laboratory scale (initial arm length $L_0 = 10$ m), 10 s and 15 s after ignition, for a junction angle $\theta = 60°$, on a horizontal terrain ($\alpha = 0$), and under a prevailing wind speed $U_W = 1$ m/s.

a quasi-constant value of I_a is obtained at steady state. For instance, for the two cases shown in Fig. 8, the junction-arm intensity was estimated (from 8 to 18 s) at about 0.35 MW/m for case 1 ($\theta = 30°$, $\alpha = 10°$, and $U_W = 0$) and at about 0.43 MW/m for case 2 ($\theta = 60°$, $\alpha = 0$, and $U_W = 0.5$ m/s).

The expression of Byram's convective number is fundamentally derived under the assumption of steady fire propagation, where a balance exists between buoyancy-driven and wind-driven forces for a fire front. Under such conditions, fire properties (ROS and fire intensity) are statistically constant during a time large enough compared to the fire residence time, allowing a quasi-equilibrium force balance to be established. For instance, the fire residence time was evaluated for the two representative cases shown in Fig. 7 by dividing the local flaming-zone width (at the fuel surface) by the corresponding local ROS. For $\theta = 30°$, $\alpha = 10°$, and $U_W = 0$, the flaming-zone width measured at $t - t_{ign} = 16$ s at the mid-arm location was approximately 0.27 m, with a local ROS of

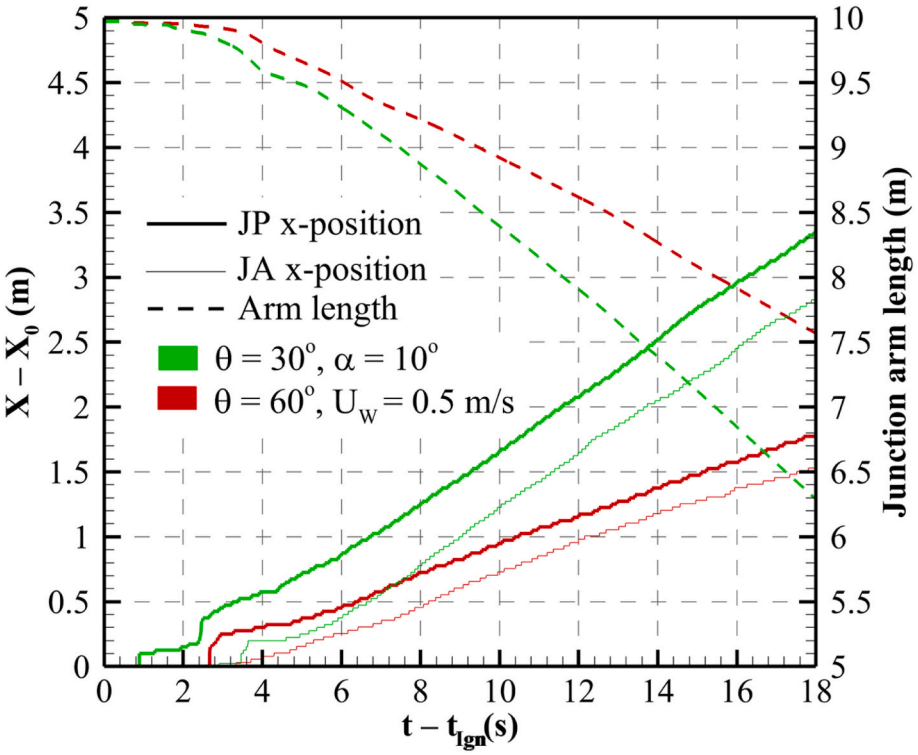

Fig. 7. Junction-point (JP) and junction-arm (JA) propagations in the x direction (X_0 being the initial position) and time evolution of the junction-arm length, obtained for shrub at laboratory scale (initial arm length $L_0 = 10$ m) and for two cases: 1 - Junction angle $\theta = 30°$, sloping terrain with $\alpha = 10°$, and no imposed wind speed ($U_W = 0$), 2 - Junction angle $\theta = 60°$, horizontal terrain ($\alpha = 0$), with a prevailing wind speed $U_W = 0.5$ m/s.

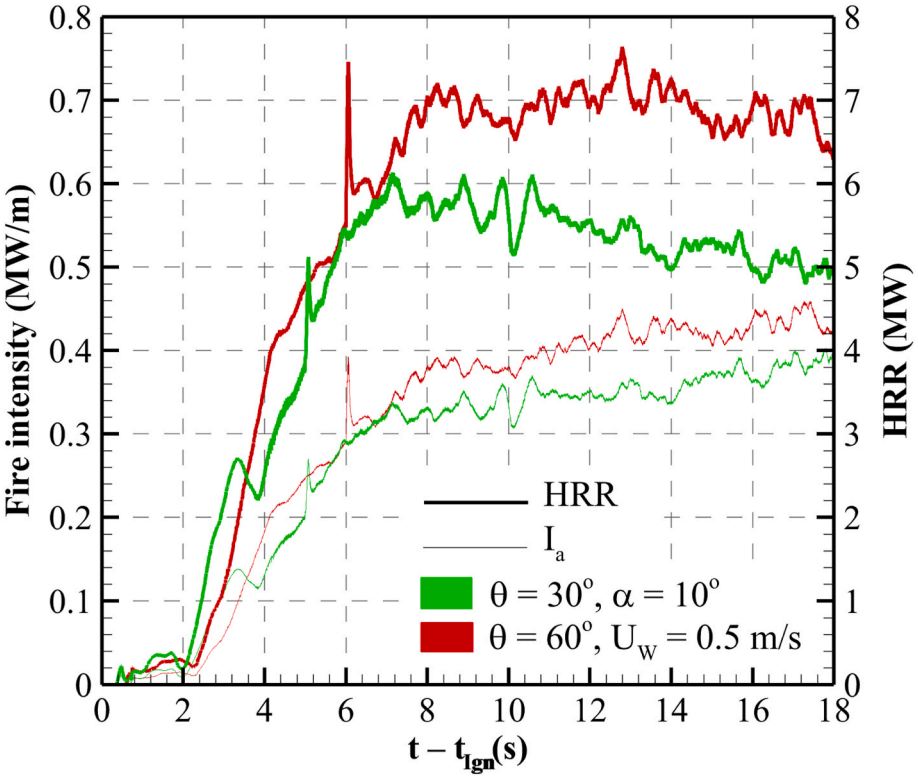

Fig. 8. Heat release rate (HRR) and junction-arm fire intensity (I_a), obtained for shrub at laboratory scale (initial arm length $L_0 = 10$ m) and for two cases: 1 - Junction angle $\theta = 30°$, sloping terrain with $\alpha = 10°$, and no imposed wind speed ($U_W = 0$), 2 - Junction angle $\theta = 60°$, horizontal terrain ($\alpha = 0$), with a prevailing wind speed $U_W = 0.5$ m/s.

0.217 m/s, yielding a residence time of about 1.24 s. For $\theta = 60°$, $\alpha = 0$, and $U_W = 0.5$ m/s, the flaming-zone width was approximately 0.25 m

and the corresponding ROS was 0.10 m/s, resulting in a residence time of about 2.5 s.

But steady propagation is not always achieved in dynamic phenomena such as junction fires, especially at small junction angle, where fire spread remains transient until the consumption of the entire fuel bed. In strongly unsteady fires, the balance between buoyancy-driven and wind-driven forces no longer holds. The fire may exhibit very irregular spread, near-simultaneous ignition of large fuel regions, or continuous acceleration with rapid growth in intensity, rather than propagation of a well-defined fire front. In these regimes, the ROS is time-dependent and the assumptions underpinning Byram's scaling break down. Hassan et al. [12] identified thresholds beyond which external environmental factors can disrupt the steadiness of junction fire propagation. This includes sudden jumps of front flame with unexpected ignitions at the end of the fuel bed [16,20,21], the final phase of junction fire when the size of the junction becomes minimal and flames fully merge, cases exhibiting abnormal increases in arm intensity (often triggered by the loss of the junction's V-shape), or rapid propagation at the upper edge of the vegetation. Fig. 9 illustrates some of these dynamics where the unburned fuel completely loses its characteristic V-shape (as shown by Fig. 9(a)) under extreme conditions with a 6 m/s applied wind, and the flaming zone covers most of the fuel bed (as shown by Fig. 9(b)). This behaviour is a clear manifestation of such extreme cases, where high wind is combined with the intensification resulting from the close proximity of converging fire fronts.

Fig. 10 shows distinct junction-arm fire intensities associated with quasi-steady and eruptive junction-fire regimes. In the quasi-steady case, the fireline intensity rapidly stabilises after ignition and remains statistically constant over time. The eruptive case shows a continuous increase in fireline intensity with no identifiable plateau. To address these challenges and obtain a correct representative ROS, a conservative approach was adopted. Irregular and eruptive cases were intentionally excluded from the present scaling analysis, and only cases exhibiting clear, quasi-steady propagation with constant junction angle were included in the scaling law assessment, ensuring that the measured ROS accurately reflects sustained fire behaviour rather than transient, irregular events. Eruptive cases will be analysed more carefully in future studies.

4.2. Junction-fire scale effect

For the same control parameters, Fig. 11 shows the effect of changing the junction initial arm length in the case of shrub and grass at laboratory and field scales. As the junction-fire scale increases, the fire HRR naturally increases; however, as shown by Fig. 11, the fire intensity of the junction arm remains practically the same across different length scales. The increase in the fire intensity observed for the junction fire with an initial junction-arm length of 5 m results actually from the final phase when the size of the junction becomes small enough for the flames to fully merge. On the other hand, the propagation of the junction point is practically unaffected by the scale of the junction. For grass vegetation, the intensity is approximately scale-invariant over the range of scales investigated, with only small deviations. This result is consistent with a field-scale experimental study of junction fires conducted with three arm lengths (47, 52, and 75 m) under identical experimental conditions [2]. The experiments revealed no significant scale effect, particularly with respect to the fundamental behaviour and dynamics of junction fires, which appear to be scale-invariant. The magnitude of ROS across the three experiments remained within the same order of magnitude, demonstrating qualitative similarity in fire development despite differences in arm length.

4.3. Junction-fires scaling law

From the junction-arm fire intensity (I_a), buoyancy characteristic velocity U_B is estimated using Eq. (2), then the effective wind speed acting in the normal direction to the junction arm ($U_{e,a}$) is obtained from Eq. (4). The ROS of the junction arm in the normal direction to the arm (R_{JA}) is obtained by multiplying the ROS of the junction arm in the x direction (obtained from Fig. 7) by sin ($\theta_{½}$). I_a, $U_{e,a}$ and R_{JA} are used to determine Byram's convective number based on the junction-arm parameters. In the case of a single, straight, quasi-infinite fire line, Eq. (3) is used to determine the Byram's number and the effective wind speed. The results of all considered cases (shrub at laboratory scale and grass at field scale) having reached a quasi-steady state of fire spread are summarised in Fig. 12. We notice first that for a given fuel type, all junction fire cases, across various slopes, wind speeds, junction angles and scales collapse onto a single scaling power-law.

This collapse can be quantified by fitting a power-law relationship of the form $R_{JA}/U_{e,a} = A\,N_C^b$ to each fuel dataset. For shrub fuel, the best-fit

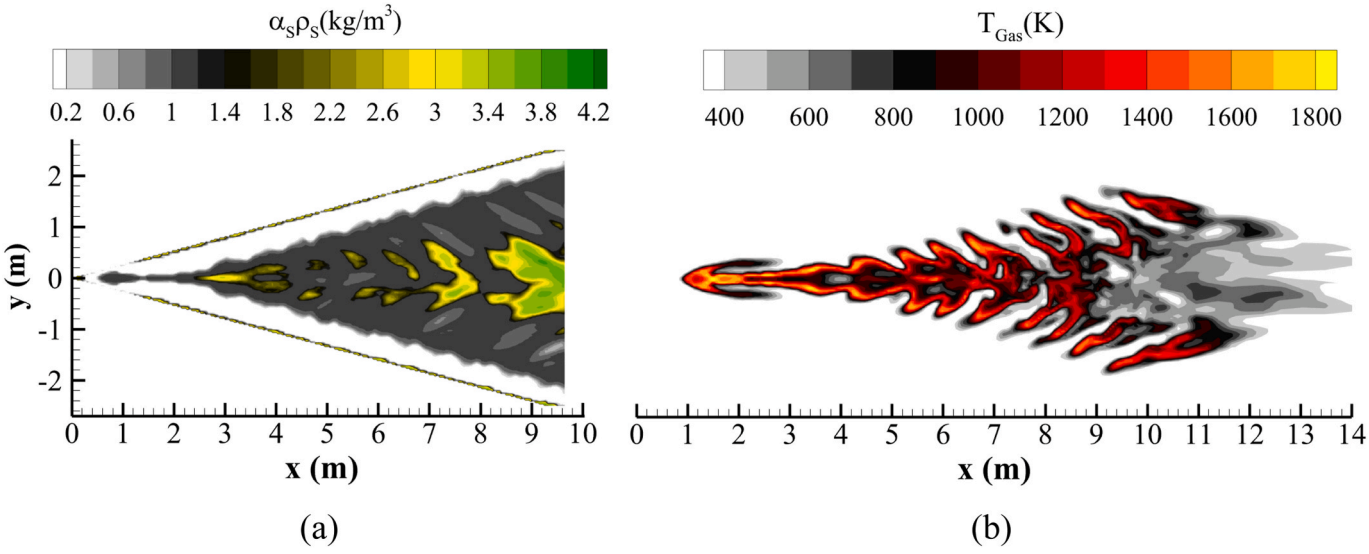

Fig. 9. Junction fire obtained 20 s after ignition for shrub at laboratory scale ($L_0 = 10$ m), for a junction angle $\theta = 60°$, on horizontal terrain ($\alpha = 0$), and for a prevailing wind speed of $U_W = 6$ m/s. (a) Distribution of fuel bulk-density at the fuel-bed surface. (b) Horizontal slice of the gas mixture temperature field at $z = 2h$ (i.e., twice the height of the vegetation).

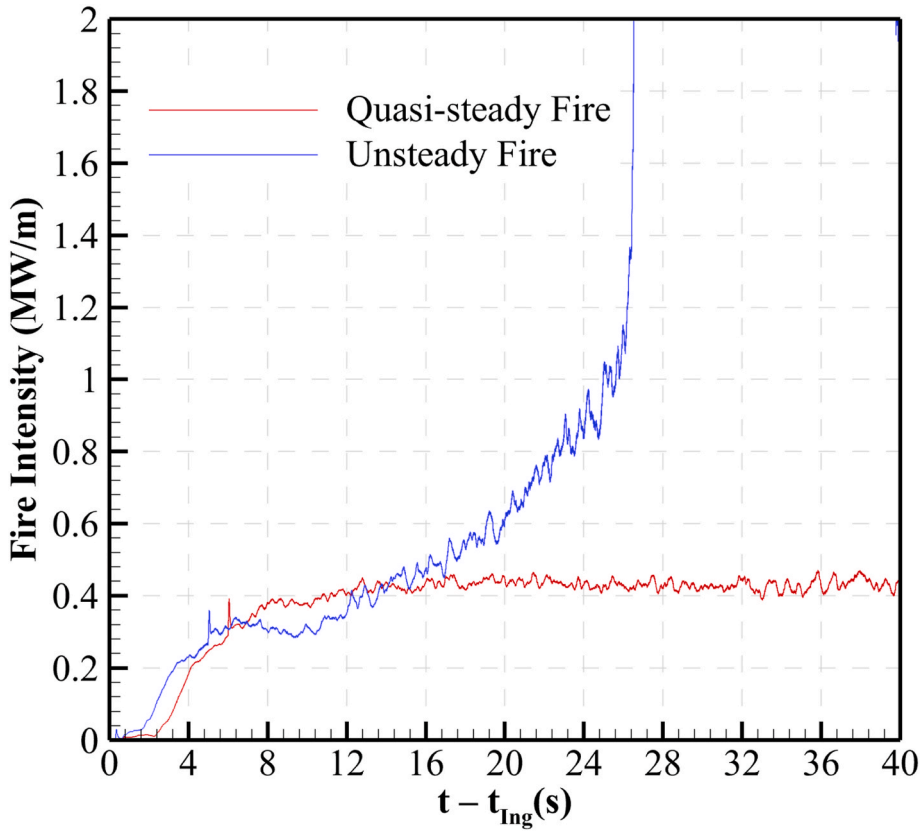

Fig. 10. Junction-arm fire intensity (I_a), obtained for shrub at laboratory scale (initial arm length $L_0 = 10$ m) and for two cases: 1 – Quasi-steady fire: Junction angle $\theta = 60°$, horizontal terrain ($\alpha = 0$), with a prevailing wind speed $U_W = 0.5$ m/s, 2 – Eruptive fire: Junction angle $\theta = 30°$, sloping terrain with $\alpha = 40°$, and no imposed wind speed ($U_W = 0$).

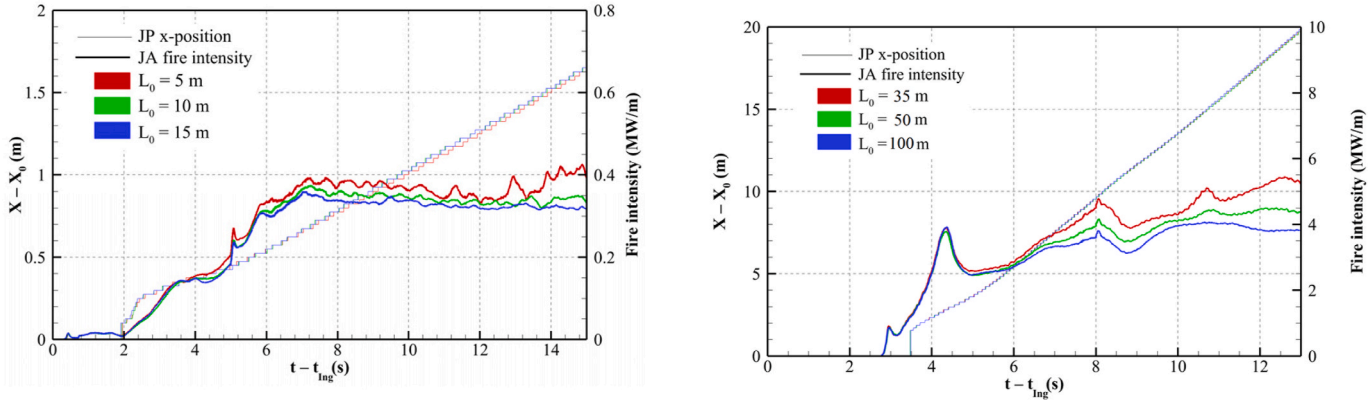

Fig. 11. Junction-point (JP) propagations in the x direction (X_0 being the initial position) and time evolution of the junction-arm (JA) fire intensity, obtained for shrub (left) for a junction angle $\theta = 60°$, for a slope angle $\alpha = 20°$, under no imposed wind ($U_W = 0$), and for three values of the initial arm length ($L_0 = 5$, 10 and 15 m), and grass (right) for a junction angle $\theta = 60°$, for a slope angle $\alpha = 40°$, under no imposed wind ($U_W = 0$), and for three values of the initial arm length ($L_0 = 35$, 50 and 100 m).

scaling is $R_{JA}/U_{e,a} = 0.0244\, N_C^{0.2767}$ with a high coefficient of determination ($R_{fit}^2 = 0.945$), indicating that most of the variance in the normalised ROS is captured by the modified convective number. For grass fuels, the fitted law is $R_{JA}/U_{e,a} = 0.2599\, N_C^{0.1153}$ ($R_{fit}^2 = 0.912$), again demonstrating strong data collapse.

Previous studies [2,3,16] showed that the smaller the junction angle the faster the junction-fire spread. The proposed scaling unifies all cases despite the intensification caused by the junction effect, encompassing the observed variations in ROS and intensity, and capturing the influence of both slope and wind on fire spread. Another important observation is the ability of the proposed scaling to merge both junction fire and straight fireline cases onto the same scaling law for each fuel type, which is not surprising since a straight fireline is a particular case of a junction fire with a junction angle $\theta = 180°$. The separation between the two fuel types is an important outcome of the obtained results and reflects the dependence of the scaling law on other fuel-related non-dimensional parameters. For instance, the expression of Byram's convective number does not account for the vegetation aerodynamic drag that depends on the drag coefficient C_d, the fuel leaf-area-index (½ α_S σ_S h) that are expected to influence the scaling law between the normalised

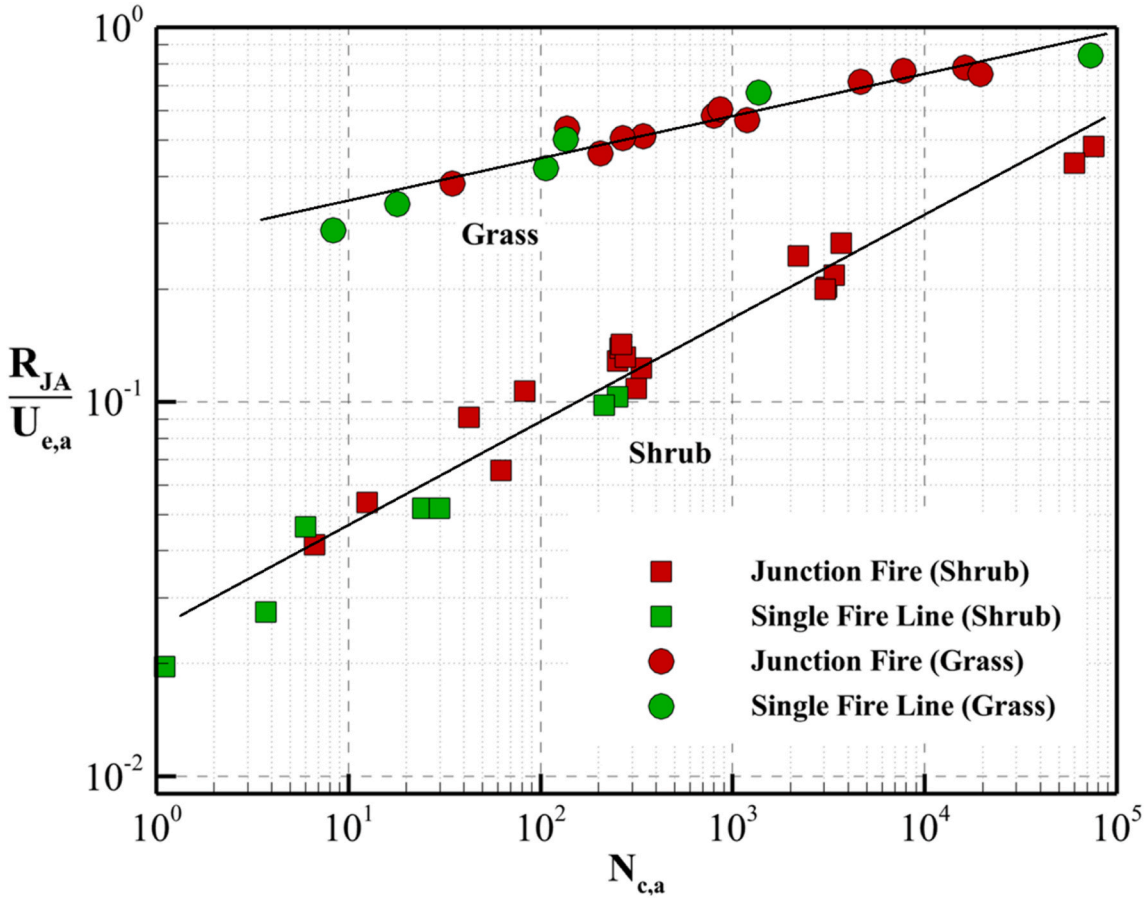

Fig. 12. Normalised junction-arm ROS in the normal direction to the arm ($R_{JA}/U_{e,a}$) versus Byram's convective number based on the junction-arm parameters, obtained for shrub at laboratory scale and for grass at field scale. Data set also includes results obtained for a single, straight, quasi-infinite fire line at both laboratory and field scales.

ROS and Byram's convective number. It should be noted that for the range of geometric and environmental parameters considered, steady-state junction-fire spread was only obtained for $N_{C,a} \gtrsim 1$, i.e., for a plume-dominated fire regime ($N_{C,a} > 10$) and for a transitional fire regime between wind/slope-driven and plume-dominated ($2 < N_{C,a} < 10$). Most of the cases with combined effects of small junction angle and relatively high wind speed or steep slope, that would have resulted in wind/slope-driven fires, did not reach a clear steady state of junction-fire spread and could not be included in the scaling law analysis. Finally, as mentioned in Section 2 and shown in Fig. 7, since $R_{JA} = R_{JP} \sin(\theta_{½})$ and since $U_{e,a} = U_e \sin(\theta_{½})$ where U_e is the effective wind speed in the junction-axis direction, the scaling law shown in Fig. 12 is also valid for the normalised ROS of the junction point R_{JP}/U_e.

5. Conclusions

This study introduced and evaluated a new scaling framework for junction fires (which propagates quasi-steadily) based on a modified expression of Byram's convective number. Through an extensive set of physics-based numerical simulations covering a wide range of scales, slopes, wind speeds, junction geometries, and two types of vegetation, the analysis has demonstrated that the proposed dimensionless formulation effectively characterises the spread of merging fires. The numerical model used to simulate junction-fire behaviour is a fully physical one that accounts for the most important phenomena occurring in a fire and has been extensively validated in different fire configurations including junction fires.

The results show that, when a junction-fire spreads quasi-steadily, the normalised ROS of a junction fire can be scaled by Byram's convective number based on the junction-arm parameters, and that this scaling depends on the fuel properties. The obtained scaling accounts for geometric (junction angle), environmental (wind speed and terrain slope), and scale (junction-arm length) parameters characterising two merging fire lines. The fact that a unified scaling law is found for both junction fires and straight quasi-infinite fire lines, yields important consequences for junction-fire research. This implies that studies carried out for straight, quasi-infinite fire-lines apply in non-dimensional form to junction fires as long as quasi-steady junction-fire spread is achieved. For instance, the dependence of the scaling law (between the normalised ROS of the junction-fire spread and Byram's convective number) on fuel properties could be investigated through a straight, quasi-infinite fire-line configuration.

The study also showed that a steady wind/slope-driven junction-fire spread is difficult to occur. The combined effect of a small junction angle and relatively severe environmental conditions (prevailing wind speed and terrain slope) often results in irregular fire spread that might have eruptive behaviour. This particular junction-fire behaviour is not yet understood and requires further studies with combined experimental and numerical approaches.

This study particularly highlights the importance of dimensional analysis in bushfire research and shows how laboratory-scale and numerical studies can provide valuable insight into the behaviour of real-world junction fires, provided that the governing non-dimensional parameters are preserved. This has many operational implications, such as improving situational awareness, supporting predictive tools for extreme fire behaviour, and enhancing firefighter safety in complex bushfire environments. Finally, the study also showed how a fundamental analysis carried out for simple fire configurations (such as a

straight, infinite fire line) can be applied to more complex scenarios. The analysis conducted in this study could be adapted to other complex configurations, such as canyon fires or fire spread under non-parallel wind and slope direction.

CRediT authorship contribution statement

Ahmad Hassan: Writing – review & editing, Writing – original draft, Visualization, Validation, Software, Resources, Project administration, Methodology, Investigation, Formal analysis, Data curation, Conceptualization. **Gilbert Accary:** Writing – review & editing, Visualization, Validation, Supervision, Software, Resources, Project administration, Methodology, Investigation, Formal analysis, Data curation, Conceptualization. **Jason Sharples:** Writing – review & editing, Visualization, Validation, Supervision, Software, Resources, Project administration, Methodology, Investigation, Formal analysis, Data curation, Conceptualization. **Khalid Moinuddin:** Writing – review & editing, Visualization, Validation, Supervision, Software, Resources, Project administration, Methodology, Investigation, Funding acquisition, Formal analysis, Data curation, Conceptualization.

Declaration of competing interest

The authors declare that they have no known competing financial interests or personal relationships that could have appeared to influence the work reported in this paper.

Acknowledgements

Aix-Marseille University computing-centre is acknowledged for granting access to its HPC resources. This work is partially funded by Natural Hazards Research Australia and Victoria University.

References

[1] D.X. Viegas, J.R. Raposo, D.A. Davim, C.G. Rossa, Study of the jump fire produced by the interaction of two oblique fire fronts. Part 1. Analytical model and validation with no-slope laboratory experiments, Int. J. Wildland Fire 21 (7) (2012) 843–856, https://doi.org/10.1071/WF10155.

[2] J.R. Raposo, et al., Analysis of the physical processes associated with junction fires at laboratory and field scales, Int. J. Wildland Fire 27 (1) (2018) 52–68, https://doi.org/10.1071/WF16173.

[3] A. Hassan, G. Accary, D. Sutherland, K. Moinuddin, Physics-based modelling of wind-driven junction fires, Fire Saf. J. 142 (2024) 104039, https://doi.org/10.1016/j.firesaf.2023.104039.

[4] R. Fox, A. McDonald, P. Pritchard (Eds.), Introduction to Fluid Mechanics, sixth ed., 2004.

[5] B. George, Forest fire behavior, in: K. Davis (Ed.), Forest Fire Control and Use, vol. 584, McGraw-Hill, New York, 1959, pp. 90–123.

[6] P.H. Thomas, The size of flames from natural fires, Symposium (International) on Combustion 9 (1) (1963) 844–859, https://doi.org/10.1016/S0082-0784(63)80091-0.

[7] P.J. Pagni, T.G. Peterson, Flame spread through porous fuels, Symposium (International) on Combustion 14 (1) (1973) 1099–1107, https://doi.org/10.1016/S0082-0784(73)80099-2.

[8] R. Nelson, Byram derivation of the energy criterion for forest and wildland fires, Int. J. Wildland Fire 3 (3) (1993) 131–138, https://doi.org/10.1071/WF9930131.

[9] R.M. Nelson, Re-analysis of wind and slope effects on flame characteristics of mediterranean shrub fires, Int. J. Wildland Fire 24 (7) (2015) 1001–1007, https://doi.org/10.1071/WF14155.

[10] D. Morvan, N. Frangieh, Wildland fires behaviour: wind effect versus Byram's convective number and consequences upon the regime of propagation, Int. J. Wildland Fire 27 (9) (2018) 636–641, https://doi.org/10.1071/WF18014.

[11] D. Morvan, G. Accary, How to properly account for slope effect in Byram's convective number? A new proposal, Fire Technology (2024), https://doi.org/10.1007/s10694-024-01670-1.

[12] A. Hassan, G. Accary, J. Sharples, K. Moinuddin, Insight into laboratory-scale junction-fire dynamics using 3-D physics-based numerical simulations, Fire Saf. J. 157 (2025) 104489, https://doi.org/10.1016/j.firesaf.2025.104489.

[13] D. Morvan, G. Accary, S. Meradji, N. Frangieh, O. Bessonov, A 3D physical model to study the behavior of vegetation fires at laboratory scale, Fire Saf. J. 101 (2018) 39–52, https://doi.org/10.1016/j.firesaf.2018.08.011.

[14] G. Accary, D. Morvan, How can CFD contribute to the understanding of wildfire behaviour? Comput. Fluid 279 (2024) 106322 https://doi.org/10.1016/j.compfluid.2024.106322.

[15] N. Frangieh, G. Accary, D. Morvan, S. Méradji, O. Bessonov, Wildfires front dynamics: 3D structures and intensity at small and large scales, Combust. Flame 211 (2020) 54–67, https://doi.org/10.1016/j.combustflame.2019.09.017.

[16] A. Hassan, G. Accary, D. Sutherland, K. Moinuddin, Physics-based modelling of junction fires: parametric study, Int. J. Wildland Fire 32 (3) (2023) 336–350, https://doi.org/10.1071/WF22121.

[17] J. Fayad, et al., Numerical study of an experimental high-intensity prescribed fire across Corsican Genista salzmannii vegetation, Fire Saf. J. 131 (2022) 103600, https://doi.org/10.1016/j.firesaf.2022.103600 (in English).

[18] A. Hassan, G. Accary, D. Sutherland, S. Méradji, K. Moinuddin, Physics-based modelling of junction fires: sensitivity and validation studies, in: D.X.V.L. M. Ribeiro (Ed.), IX International Conference on Forest Fire Research, 2022, pp. 315–322, https://doi.org/10.14195/978-989-26-2298-9_50. Coimbra, Portugal.

[19] D. Morvan, Physical phenomena and length scales governing the behaviour of wildfires: a case for physical modelling, Fire Technol. 47 (2) (2011) 437–460, https://doi.org/10.1007/s10694-010-0160-2.

[20] D. Viegas, J. Raposo, A. Figueiredo, Preliminary analysis of slope and fuel bed effect on jump behavior in forest fires, Procedia Eng. 62 (2013) 1032–1039, https://doi.org/10.1016/j.proeng.2013.08.158.

[21] B. Holyland, B. Cirulis, T.D. Penman, A.I. Filkov, The effects of junction fire development on thermal behaviour at the field scale, Fire Saf. J. 143 (2024) 104057, https://doi.org/10.1016/j.firesaf.2023.104057.